blood®
Regular Article

THROMBOSIS AND HEMOSTASIS

Structure of an extended β_3 integrin

Dongwen Zhou,[1] Aye Myat Myat Thinn,[1,2] Yan Zhao,[1,3] Zhengli Wang,[1] and Jieqing Zhu[1,2]

[1]Blood Research Institute, BloodCenter of Wisconsin, part of Versiti, Milwaukee, WI; [2]Department of Biochemistry, Medical College of Wisconsin, Milwaukee, WI; and [3]Department of Physiology, School of Basic Medical Science, Shanghai University of Traditional Chinese Medicine, Shanghai, China

KEY POINTS

- **Conformational extension is essential for integrin to fulfill its cell-adhesion function in platelet-mediated hemostasis and thrombosis.**
- **High-resolution structures of β_3 integrin in intermediate and extended conformations reveal atomic-level conformational rearrangements.**

Cells use adhesion receptor integrins to communicate with their surroundings. Integrin activation and cellular signaling are coupled with change from bent to extended conformation. β_3 integrins, including $\alpha_{IIb}\beta_3$, which is essential for the function of platelets in hemostasis and thrombosis, and $\alpha_V\beta_3$, which plays multiple roles in diverse cell types, have been prototypes in understanding integrin structure and function. Despite extensive structural studies, a high-resolution integrin structure in an extended conformation remains to be determined. The human β_3 Leu33Pro polymorphism, located at the PSI domain, defines human platelet-specific alloantigens 1a and 1b (HPA-1a/b), immune response to which is a cause of posttransfusion purpura and fetal/neonatal alloimmune thrombocytopenia. Leu33Pro substitution has also been suggested to be a risk factor for thrombosis. Here we report the crystal structure of the β_3 headpiece in either Leu33 or Pro33 form, both of which reveal intermediate and fully extended conformations coexisting in 1 crystal. These were used to build high-resolution structures of full-length β_3 integrin in the intermediate and fully extended states, agreeing well with the corresponding conformations observed by electron microscopy. Our structures reveal how β_3 integrin becomes extended at its β-knee region and how the flexibility of β-leg domains is determined. In addition, our structures reveal conformational changes of the PSI and I-EGF1 domains upon β_3 extension, which may affect the binding of conformation-dependent anti–HPA-1a alloantibodies. Our structural and functional data show that Leu33Pro substitution does not directly alter the conformation or ligand binding of β_3 integrin. (*Blood*. 2018;132(9):962-972)

Introduction

Integrins are a family of 24 α/β heterodimeric adhesion receptors that transmit bidirectional signals across the cell membrane.[1] Each integrin subunit contains a large extracellular domain composed of a headpiece and leg piece, a transmembrane domain, and usually a short cytoplasmic tail (supplemental Figure 1, available on the *Blood* Web site).[2] The α headpiece consists of β-propeller and thigh domains and an inserted αI domain on top of the β-propeller in a subset of α subunits, such as leukocyte-specific α_L. The α leg piece includes calf-1 and –2 domains. The β headpiece contains βI, hybrid, PSI, and I-EGF1 domains (Figure 1A). The β leg piece contains I-EGF2 to -4 and β-tail domains (Figure 1A). Structural studies in the last 17 years, largely based on β_3 integrins, including $\alpha_{IIb}\beta_3$ and $\alpha_V\beta_3$,[3-11] have greatly advanced our understanding of integrin conformational regulation upon activation. Platelet-specific $\alpha_{IIb}\beta_3$ plays an essential role in hemostasis and thrombosis,[12] and $\alpha_V\beta_3$ is important for the growth and survival of many cell types.[13,14] In the resting state, integrin adopts a bent conformation, with the headpiece folded onto the leg piece (supplemental Figure 1A). Crystallographic and electron microscopy (EM) studies of $\alpha_{IIb}\beta_3$ and $\alpha_V\beta_3$ have revealed 2 major conformational rearrangements: the swing-out motion of the hybrid domain, resulting in headpiece opening, and the switchblade-like movement of the headpiece from the leg domains, leading to integrin extension and leg separation (supplemental Figure 1B-C).[2,7] Despite the visualization of β_3 extension by EM at low resolution (supplemental Figure 1B-C), a high-resolution extended β_3 structure is not available.

A Leu33Pro polymorphism at the β_3 PSI domain defines the human platelet-specific alloantigen 1 (HPA-1) system.[15] Mismatched HPA-1a/b (Leu33/Pro33) is a major cause of 2 severe bleeding disorders: fetal/neonatal alloimmune thrombocytopenia and posttransfusion purpura, which result from the generation of anti–HPA-1a alloantibodies.[16,17] In addition, whether the Pro33 variant enhances β_3 activity, as a risk factor for thrombosis, is controversial.[18-20] It is unknown whether Leu33Pro substitution affects the conformation of the PSI domain, which undergoes outward movement along with headpiece opening and extension.

Crystallographic studies of a full-length extended integrin have not been successful. This is largely due to the flexibility of the β-leg domains in the extended conformation as indicated by EM studies.[2] In our study, to obtain the high-resolution crystal structure of an extended β_3 integrin, we engineered a cβ_3

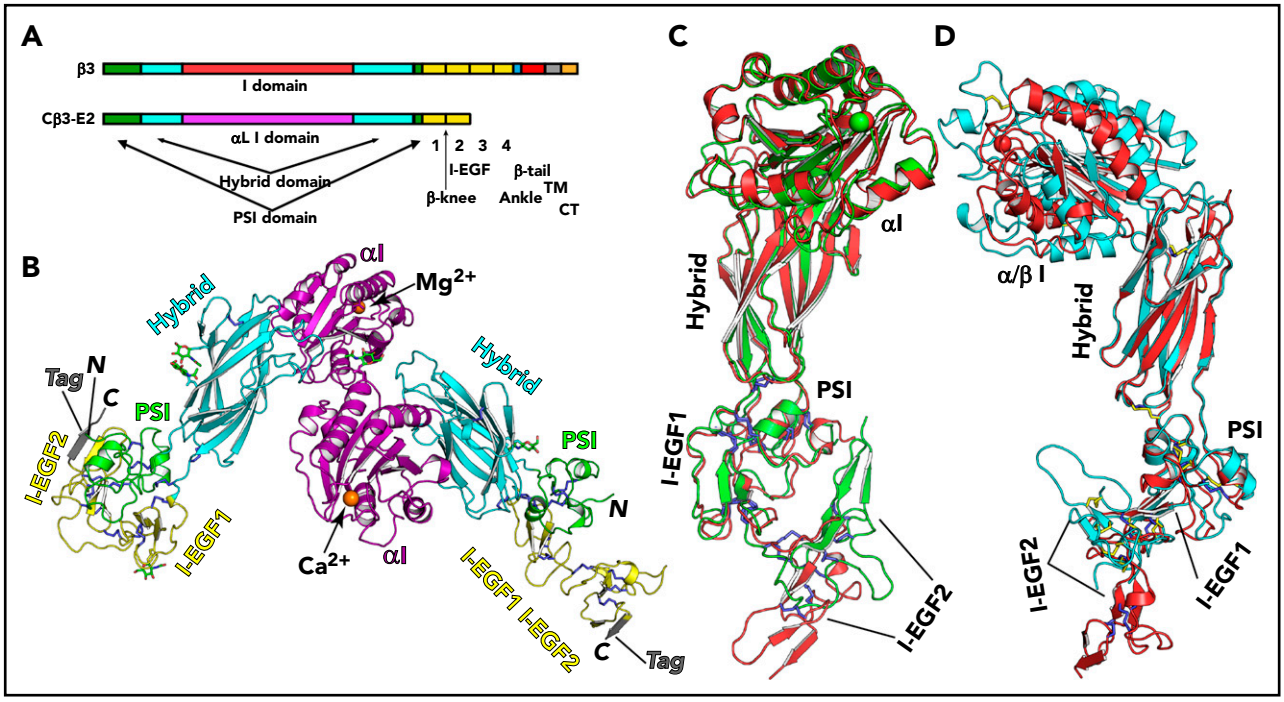

Figure 1. Overall structure of the single-chain chimeric β_3 headpiece. (A) Diagram of the native and chimeric β_3 ($c\beta_3$) constructs. The $c\beta_3$-E2 construct was truncated at the I-EGF2 domain. (B) The 2 copies of $c\beta_3$-E2 structure in the asymmetric unit. N-linked glycans are shown as sticks with green carbons, red oxygens, and blue nitrogens. Metal ions are shown as spheres. Disulfide bonds are blue sticks. (C) Structural alignment of the 2 $c\beta_3$-E2 molecules in the asymmetric unit. (D) Structural comparison of the extended $c\beta_3$-E2 structure (in red; disulfide bonds in blue) with the native β_3 structure (PDB 3FCS; in cyan; disulfide bonds in yellow). The 2 structures were aligned on the hybrid domain.

fragment containing the headpiece and β-knee region at where β_3 becomes extended. $c\beta_3$ could be expressed without an α subunit. We solved the crystal structures of the $c\beta_3$ fragment in both Pro33 and Leu33 forms. The structures revealed intermediate and fully extended β_3 conformations at the β knee, providing high-resolution information on how β_3 becomes extended. The structures of full-length β_3 integrin were built in both intermediate and fully extended conformations, agreeing well with the corresponding conformations observed by EM. Our structural and functional studies provide an atomic-level understanding of integrin conformational regulation on the cell surface.

Methods

DNA constructs

The α_{IIb}, α_V, α_L, α_5, β_1, β_2, β_3, and EGFP-talin head constructs were as described previously.[21-23] Mutations were generated by the QuikChange XL Site-Directed Mutagenesis Kit (Agilent Technologies). The $c\beta_3$ construct was designed by replacing the β_3 βI domain (residues Tyr110-Gly349) with the α_L αI domain (residues Gly128-Lys304). The full-length $c\beta_3$ DNA construct was generated by overlapping polymerase chain reaction and cloned into the pcDNA3.1/Myc-His$^+$ A vector using *HindIII* and *XbaI* restriction sites. The DNA fragment of the $c\beta_3$ headpiece containing the PSI with either Pro33 or Leu33, hybrid, αI, I-EGF1, and I-EGF2 domains was cloned into the *XhoI* and *MluI* sites of the ExpressTag 1 vector, which was based on the pIRES2-EGFP vector.[24] The construct was C-terminal tagged with an HRV 3C protease cleavage site, protein C epitope, hexahistidine, and streptavidin binding protein affinity tag. All constructs were validated by DNA sequencing.

Protein expression and purification

The $c\beta_3$ headpiece construct was transfected into HEK293S GnTI$^-$ cells. The transfected cells were cultured in a medium containing 1 mg/mL of G418 for at least 10 days before a pool of EGFP$^+$ cells were sorted. The EGFP$^+$ cells were cultured in roller bottles in the selection medium. The cell-culture supernatant was collected every 3 to 5 days. The $c\beta_3$ headpiece proteins were purified from the supernatant using Strep-Tactin Superflow Plus beads following the manufacturer's protocol (Qiagen). The proteins were treated with HRV 3C protease to remove the tags and then with Endoglycosidase H to remove the high-mannose type of N-linked glycans. The untagged proteins were finally purified with a Superdex 200 column (GE Healthcare) equilibrated with a buffer containing 20 mM of Tris-hydrochloride (potential of hydrogen [pH], 7.5), 150 mM of sodium chloride (NaCl), 1 mM of calcium chloride, and 1 mM of magnesium chloride and concentrated to 10 mg/mL for protein crystallization.

Protein crystallization and crystallography

Crystallization was performed at 4°C by hanging-drop vapor diffusion method with 1:1 volume/volume ratio of protein and cocktail solutions. Both Pro33 and Leu33 forms of $c\beta_3$ headpiece proteins were crystallized in either 20% PEG 6000 plus 0.1 M of Tris-hydrochloride (pH, 8.5) or 12% PEG 8000 plus 0.2 M of NaCl and 0.1 M of *N*-2-hydroxyethylpiperazine-*N*′-2-ethanesulfonic acid (pH, 7.5). The crystals were cryoprotected with additional glycerol in the 18% PEG 8000 solution in 5% increments up to 20% final concentration. For dehydration, crystals were soaked in the 18% PEG 8000 solution containing 2 M of NaCl and 20% glycerol at 4°C for >3 days before being flash frozen in a pool of liquid nitrogen.

Crystal X-ray diffraction data were collected at the APS LS-CAT beamline 21-ID-F and processed with iMosflm.[25] The structure was solved by molecular replacement with PHASER[26] using the α_L αI domain crystal structure (PDB 3F74) as a search model. The structures were manually built in *Coot*[27] and refined using PHENIX.REFINE.[28] The atomic coordinates and structural factors have been deposited in the protein data bank under accession numbers 6BXF (for β_3-Leu33), 6BXB (for β_3-Pro33 after dehydration), and 6CKB (for β_3-Pro33 before dehydration).

Ligand and conformation-specific antibody binding assay

The ligand mimetic PAC-1 (BD Biosciences), human fibronectin (Sigma-Aldrich) labeled with Alexa Fluor-647, and human ICAM-1 with a C-terminal Fc tag (expressed as a secreted protein in HEK293FT cells) were used as ligands for $\alpha_{IIb}\beta_3$, $\alpha_V\beta_3$, and $\alpha_L\beta_2$, respectively. 9EG7 (BD Biosciences) is a rat anti-β_1 mAb that reports β_1 integrin extension.[29,30] Both Alexa Fluor-647–labeled fibronectin and 9EG7 were used for measuring the activation of $\alpha_5\beta_1$ integrin. The ligand or monoclonal antibody (mAb) binding assay using integrin-transfected HEK293FT cells was performed as described previously in the presence of integrin inhibitor Ca^{2+}/Mg^{2+} (1 mM) or Ca^{2+} (0.2 mM) plus Mn^{2+} (2 mM).[21-23] The binding of ligand or conformation-specific mAb was presented as the mean fluorescence intensity normalized to the mean fluorescence intensity of integrin expression reported by the mAbs AP3, TS2/4, and MAR4 for β_3, $\alpha_L\beta_2$, and $\alpha_5\beta_1$, respectively.

Results

Design of a single-chain cβ$_3$ headpiece construct

The βI and αI domains are structural homologs.[31] The αI but not βI domains can be expressed autonomously.[32-34] By replacing the βI with the αI domain of α_L integrin, the cβ subunit could be expressed as a single-chain construct independent of an α subunit (A.M.M.T., Z.W., D.Z., Y.Z., Brian R. Curtis, and J.Z., manuscript submitted April 2018). We solved the crystal structure of the single-chain cβ$_3$ ectodomain that adopts a bent conformation resembling β_3 in the $\alpha_{IIb}\beta_3$ or $\alpha_V\beta_3$ complex (A.M.M.T., Z.W., D.Z., Y.Z., Brian R. Curtis, and J.Z., manuscript submitted April 2018). In the bent conformation of the β_3 subunit, the headpiece folds onto the lower leg domains, forming close contacts between the hybrid and I-EGF3 to -4 domains (supplemental Figure 1A).[4,5] Such interactions help maintain β_3 in the bent conformation even in the absence of an α subunit (A.M.M.T., Z.W., D.Z., Y.Z., Brian R. Curtis, and J.Z., manuscript submitted April 2018) and upon disruption may facilitate integrin extension. The β integrin extension occurs at the I-EGF1/2 junction, denoted as β knee (supplemental Figure 1B-C; Figure 1A).[2] We generated a cβ$_3$ headpiece construct containing the PSI, hybrid, αI, I-EGF1, and I-EGF2 domains, namely cβ$_3$-E2 (Figure 1A). In the absence of the restrains of the lower leg domains, we expected cβ$_3$-E2 might adopt an extended conformation. To investigate whether the Leu33Pro polymorphism affects the β_3 conformation, both Leu33 and Pro33 forms of cβ$_3$-E2 were prepared.

Two conformations of a single-chain cβ$_3$ headpiece coexist in 1 crystal

Both Leu33 and Pro33 forms of cβ$_3$-E2 crystals belong to the same space group (Table 1). The original crystals diffracted X-ray up to 2.8-Å resolution, which was improved by crystal dehydration. The unit cell was shortened in 1 dimension after dehydration (Table 1), as a result of more tightly packed crystal lattice (supplemental Figure 2A). The cβ$_3$-E2-Pro33 structure obtained after crystal dehydration was refined to a resolution of 2.39 Å, with an R_{free} of 0.267. The cβ$_3$-E2-Pro33 structure obtained without crystal dehydration was refined to a resolution of 2.80 Å, with an R_{free} of 0.296. The cβ$_3$-E2-Leu33 structure was obtained with the crystals without dehydration and was refined to a resolution of 3.2 Å, with an R_{free} of 0.335 (Table 1). Two cβ$_3$-E2 molecules are present per asymmetric unit (Figure 1B).

All the domains in the cβ$_3$-E2 structure are well resolved in both molecules of the asymmetric unit (Figure 1B). As seen in the isolated αI structures, either Mg^{2+} or Ca^{2+} occupies the metal-ion–dependent adhesion site (Figure 1B). The remaining residues of the C-terminal tag after 3C protease cleavage form an antiparallel β-sheet interaction with the I-EGF2 domain (Figure 1B). Structural superimposition shows that the 2 molecules share similar conformations at the αI, hybrid, and PSI domains but have remarkably distinct conformations at the junction of I-EGF1 and I-EGF2 domains (Figure 1C). One molecule adopts an extended confirmation, whereas the other shows a bent-like conformation (Figure 1C). When compared with the native β_3 headpiece structures, cβ$_3$-E2 resembles the closed rather than open headpiece conformation (Figure 1D). However, when superimposed onto the αI domain of the cβ$_3$ ectodomain crystal structure (A.M.M.T., Z.W., D.Z., Y.Z., Brian R. Curtis, and J.Z., manuscript submitted April 2018), a slight swing-out of the hybrid domain was observed (supplemental Figure 3A-B). This was associated with the downward displacement of the α7 helix C-terminus (supplemental Figure 3A-B). Nonetheless, the αI domain of cβ$_3$-E2 was in a low-affinity conformation, as seen in the cβ$_3$ ectodomain crystal structure (supplemental Figure 3A-B).

These structural features were observed in both cβ$_3$-E2-Leu33 and cβ$_3$-E2-Pro33 crystals. No significant structural differences were observed between these 2 isoforms of cβ$_3$-E2 (supplemental Figure 4A-D). Therefore, the Pro33 form was used to represent the cβ$_3$-E2 structure, because it gave a higher resolution than the Leu33 form (Table 1). Of note, the 2 cβ$_3$-E2 molecules in the asymmetric unit packed closer to each other after crystal dehydration (supplemental Figure 2B-C), but no significant conformational changes were observed after dehydration (supplemental Figure 2B-C).

β_3 extension at the I-EGF1/I-EGF2 junction

As expected, we observed an extended conformation at the I-EGF1/I-EGF2 junction in the cβ$_3$-E2 structure. In the crystal lattice, the I-EGF2 domain of 1 molecule of the asymmetric unit was free of crystal contact and thus had enough room to adopt an extended conformation (supplemental Figure 2A). Remarkably, the I-EGF2 domain of the other molecule of the asymmetric unit was trapped in the bent-like conformation by the close lattice contacts with its neighboring symmetry mates (supplemental Figure 2A). When superimposed with the bent native β_3 structure based on either the I-EGF1 or I-EGF2 domain (Figure 2A), the bent-like conformer observed in the cβ$_3$-E2 structure actually exhibits an intermediate state in between the fully bent and fully extended conformations (Figure 2A). Therefore, we captured a snapshot of β_3 integrin on the pathway from the bent to extended conformational transition.

Each of the integrin I-EGF domains contains 8 cysteines that form disulfide bonds in the pattern of C1-C5, C2-C4, C3-C6, and

Table 1. Statistics of X-ray diffraction data and structure refinement

Data collection	cβ3-E2-P33		cβ3-E2-L33
	Before dehydration	After dehydration	No dehydration
Space group	$P2_1$	$P2_1$	$P2_1$
Unit cell			
a, *b*, *c*, Å	59.08, 80.91, 126.72	59.56, 79.84, 116.16	59.07, 81.47, 127.96
α, β, γ, °	90.0, 96.4, 90.0	90.0, 91.42, 90.0	90.0, 97.1, 90.0
Wavelength, Å	0.97872	0.97872	0.97872
Resolution, Å	2.80	2.39	3.20
R_{merge}, %*†	15.0 (>100)	13.8 (>100)	22.6 (>100)
No. of reflections, measured/unique	222 851/29 474	328 778/43 236	152 292/20 112
$I/\sigma(I)$*	8.6 (0.5)	9.6 (0.7)	6.5 (0.6)
Completeness, %*	100 (100)	99.7 (98.8)	100 (100)
Redundancy*	7.6 (7.6)	7.6 (6.8)	7.6 (7.6)
CC1/2*	0.995 (0.118)	0.996 (0.121)	0.959 (0.134)
Refinement			
Resolution, Å	2.80	2.39	3.20
Unique reflections, work/free	29 394/1 479	43 143/2 128	20 063/1 019
R_{work}/R_{free}‡	0.242/0.296	0.219/0.267	0.265/0.335
No. of atoms, protein/carbohydrates/water	7 223/70/4	7 215/70/170	7 197/98/8
Molecules per asymmetric unit	2	2	2
RMSD from ideal			
Bond lengths, Å	0.009	0.004	0.003
Bond angles, °	1.052	0.650	0.625
Ramachandran plot, favored/allowed/outliers, %	87.57/10.81/1.62	92.64/7.14/0.22	87.87/9.75/2.38
PDB code	6CKB	6BXB	6BXF

PDB, Protein Data Bank; RMSD, root mean square deviation.

*The highest-resolution shell is shown in parentheses.

†$R_{merge} = \sum_h\sum_i|I_i - \langle I\rangle|/\sum_h\sum_i I_i$, where I_i is the observed intensity of the i-th measurement of reflection h, and ⟨I⟩ is the average intensity of that reflection obtained from multiple observations.

‡$R = \sum||F_o| - |F_c||/\sum|F_o|$, where F_o and F_c are the observed and calculated structural factors, respectively, calculated for all data. R_{free} is the *R* value obtained for a test set of reflections consisting of a randomly selected ~5% subset of data excluded from refinement.

C7-C8, except the I-EGF1 domain[5] (Figure 2B). The C1-C5 disulfide bond and C1-C2 (C473-C486 of β_3) loop of the I-EGF2 domain are pivotal in the transition from the bent to extended conformation at the I-EGF1/2 junction (Figure 2B-D). The C1-C2 loop of I-EGF2 was incompletely defined in the bent $\alpha_{IIb}\beta_3$ and 1 of the bent $\alpha_V\beta_3$ structures as a result of the lack of complete electron density, but a complete backbone conformation was relatively well defined in another bent $\alpha_V\beta_3$ structure (supplemental Figure 5A-C).[4,5,35] In our intermediate cβ3-E2 structure, the strong electron density allowed us to build a complete conformation for both the backbone and side chains of the C1-C2 loop in the I-EGF2 domain (supplemental Figure 5D). We were also able to build a complete backbone conformation of the C1-C2 loop in the extended I-EGF2 domain, although some of the side chain conformations were not well defined because of the weak electron density (supplemental Figure 5E). Structural superimposition on the I-EGF2 domain revealed the extension of I-EGF1 afforded by the conformational rearrangement of the flexible C1-C2 loop and rotational movement at the C1 position (Figure 2B-D).

In the bent conformation, the Cα-Cα distance between the N-terminal C435 of I-EGF1 and the C-terminal E522 of I-EGF2 was 25.3 Å (Figure 2B). This distance changed to 33.6 Å in the intermediate conformation (Figure 2C) and to 45 Å in the extended conformation (Figure 2D). In coordination with these changes, the Cα-Cα distance between the C1 and C2 residues changed from 16.9 Å in the bent, to 14.9 Å in the intermediate, and to 13.8 Å in the extended states (Figure 2B-D). Along with the extension of the I-EGF1/2 junction, there was a rotational movement of the I-EGF1 domain using the C1-C5 disulfide bond as a hinge. There were large conformational rearrangements for both backbone and side chains of the I-EGF2 C1-C2 loop during the I-EGF1 extension (Figure 2B-D; supplemental Figure 4). The rotation of the C1-C5 disulfide bond of I-EGF2 accompanied with the swinging of the C1-C2 loop (Figure 2B-D). Interestingly, a small portion of the C1-C2 loop at the C2 end became α helical in the extended conformation (Figure 2D). No disulfide bond exchange was observed. All the disulfide bonds of I-EGF1 and I-EGF2 domains remained the same as in the bent conformation during the I-EGF1 extension (Figure 2B-D).

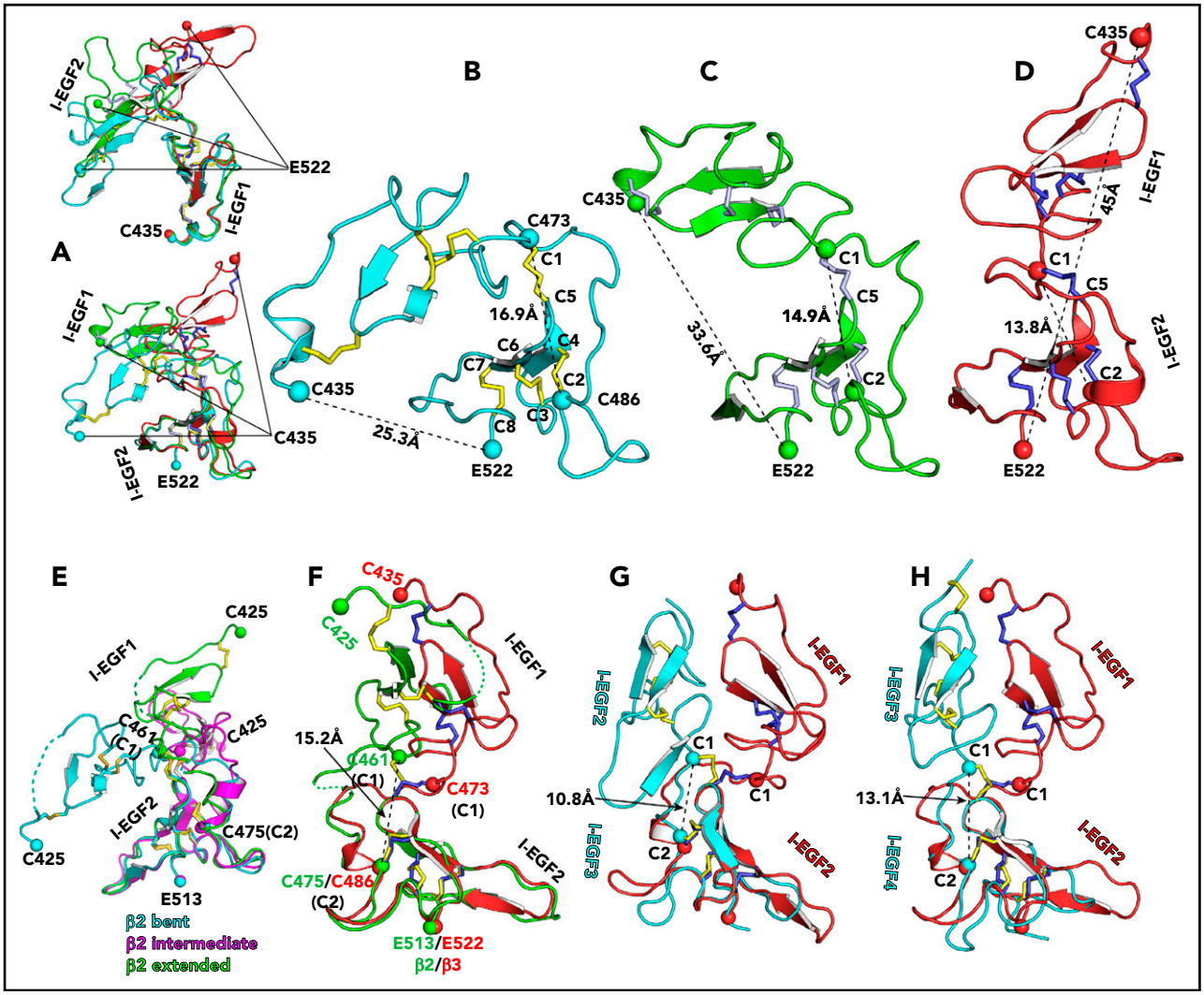

Figure 2. β_3 integrin extension at the I-EGF1/I-EGF2 junction. (A) Structural superposition of the cβ_3-E2 I-EGF1-2 domains on the I-EGF1 (upper) or the I-EGF2 (lower) domain of the bent native β_3 structure (PDB 4G1M). (B-D) The 3 structures are shown separately after being superimposed on the I-EGF2 domains. The bent (B), intermediate (C), and extended (D) forms are shown in cyan, green, and red, respectively. Disulfide bonds are sticks. Residues of interest are shown as Cα spheres. The 8 cysteines of the I-EGF2 domain are numbered. (E) Structural superposition on the I-EGF2 of the bent (PDB code 4NEH), intermediate (PDB 2V26), and extended (PDB 2V28) I-EGF1-2 domains of β_2 integrin. (F) Structural superposition on I-EGF2 of the extended I-EGF1-2 domains of β_3 (red) and β_2 (green) integrins. (G-H) Structural comparison of the extended β_3 I-EGF1-2 (PDB 6BXB) with the β_3 I-EGF2-3 (G; PDB 3FCS) or I-EGF3-4 (H; PDB 3FCS) domains. The I-EGF3 or I-EGF4 domain was superimposed onto the I-EGF2 domain.

Two crystal structures of β_2 fragments were determined previously.[36] One contains the PSI, hybrid, and I-EGF1-2 domains and is bent at the I-EGF1/2 junction. The other contains an extra I-EGF3 domain and exhibits an extended I-EGF1/2 junction. When superimposed onto the I-EGF2 domain of the β_2 ectodomain structure in the bent conformation,[37] the bent β_2 fragment, in fact, showed an intermediate conformation, in which the I-EGF1 orientated close to the extended state (Figure 2E). Compared with our extended β_3 headpiece, the I-EGF1 in the extended β_2 fragment was in a less straight position relative to the I-EGF2 domain (Figure 2F). The Cα-Cα distance between I-EGF2 C1 (C461) and C2 (C475) was 15.2 Å, which was longer than that of the extended β_3 (Figure 2D). An α-helical conformation at the C2 end of the β_2 I-EGF2 C1-C2 loop presented at both the bent and intermediate states, but it became less α helical in the extended state (Figure 2E-F).

Extended structure of β_3 integrin

Previous crystallographic studies have determined the crystal structures of β_3 ectodomain in the bent conformation and β_3 headpiece (containing βI, hybrid, PSI, and I-EGF1 domains) either in the closed or open conformation.[4-6,38] Of note, EM studies have suggested that the integrin headpiece extends away from the leg domains on the cell surface, either remaining in the closed conformation, the same as in the bent state, or becoming an open configuration.[7,8,11] However, the conformations of I-EGF2-4 and β-tail domains likely remain unchanged after headpiece extension and leg separation, as shown by the EM structures. Our current cβ_3-E2 crystal structures revealed the extension of β_3 at the I-EGF1/I-EGF2 junction. Using our intermediate and extended I-EGF1/I-EGF2 structures as templates, and by superimposing the β_3 headpiece structure onto the I-EGF1 domain and superimposing the I-EGF2-4 and β-tail structures onto the I-EGF2 domain, we were able to build a complete high-resolution structure of β_3 ectodomain at both the intermediate and extended conformations (Figure 3A-D).

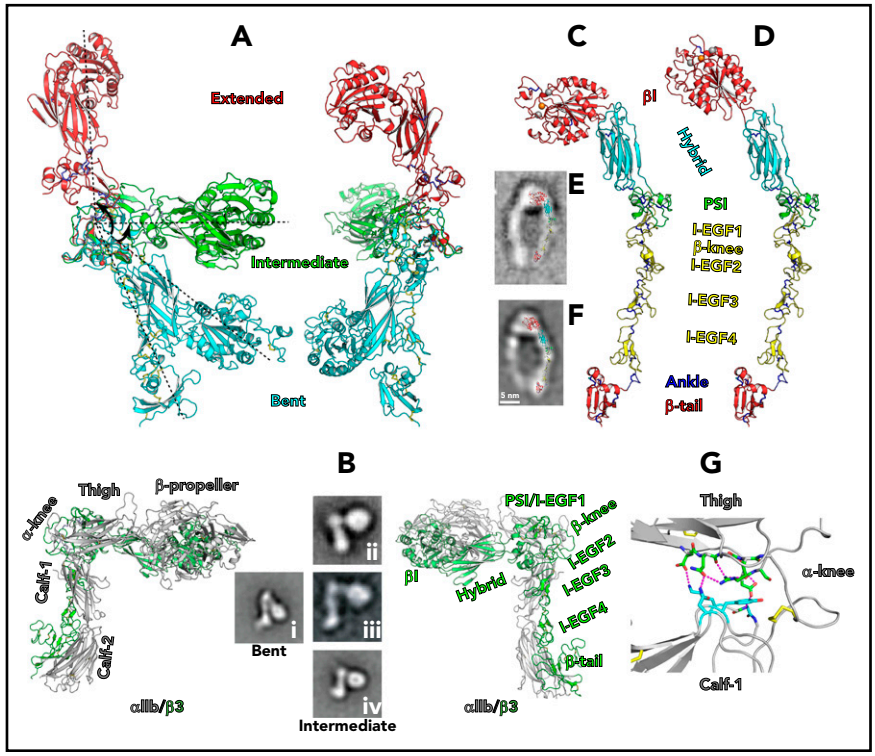

Figure 3. Extended structure of β_3 integrin. (A) Two different views of the intermediate (green) and extended (red) cβ_3-E2 structures superimposed on the I-EGF2 domain of the bent (cyan) native β_3 structure (PDB 4G1M). (B) Intermediated (half-extended) conformation of $\alpha_{IIb}\beta_3$. The structure was built based on the intermediated conformation of I-EGF1-2 and shown in 2 views. The negative staining EM images shown are full-length $\alpha_{IIb}\beta_3$ (i),[11] ectodomain of $\alpha_V\beta_3$ (ii),[7] ectodomain of $\alpha_{IIb}\beta_3$ (iii),[5] and full-length $\alpha_{IIb}\beta_3$ (iv).[11] The images were not shown in the same scale. (C-D) Modeled extended β_3 structure with closed (C) or open (D) headpiece. The model was generated by the superimposition of the extended cβ_3-E2 structure onto the I-EGF2 domain of the native β_3 structure first and then superimposition of the closed or open β_3 headpiece structure onto the hybrid domain of the cβ_3-E2 structure. (E-F) Overlay of the extended β_3 structure with the EM image of extended $\alpha_V\beta_3$[7] with closed headpiece (E) or extended $\alpha_{IIb}\beta_3$ with open headpiece[11] (F). (G) α_{IIb} thigh/calf-1 interface at the bent conformation (PDB 3FCS). Interfacial residues are shown as sticks with green and cyan carbons for thigh and calf-1 domains, respectively. Hydrogen bonds are dashed in magenta. Disulfide bonds are yellow sticks. Panels Bi, Biv, and F reprinted from Eng et al[11] with permission; panels Bii and E are reprinted from Takagi et al[7] with permission; and panel Biii is reprinted from Zhu et al[5] with permission.

At the intermediate state, the β_3 headpiece extended halfway to the fully extended conformation (Figure 3A). In addition to the acute bent conformation (Figure 3Bi), the intermediate conformations of $\alpha_V\beta_3$ (Figure 3Bii) and $\alpha_{IIb}\beta_3$ complexes (Figure 3Biii-iv) were observed by the EM studies.[5,7,11] At this intermediate state, the leg domains were still associated with each other, as in the bent conformation, and the headpiece remained closed. The structural model of the α_{IIb} subunit at the intermediate conformation was built by the structural superimpositions of the closed $\alpha_{IIb}\beta_3$ headpiece and the associated $\alpha_{IIb}\beta_3$ leg domains onto the modeled intermediated β_3 subunit with the closed headpiece (Figure 3B). Remarkably, this structural model of $\alpha_{IIb}\beta_3$ in the intermediate conformation agreed well with the intermediate EM structures (Figure 3B), demonstrating the reliability of our structure.

On the basis of the extended cβ_3-E2 structure, we built the extended structure of the β_3 ectodomain with either the closed (Figure 3C) or the open (Figure 3D) headpiece conformation. Similar to the intermediate conformation of β_3, the extended structures of β_3 fit near perfectly into the EM structures of extended β_3 with a closed or open headpiece (Figure 3E-F), again demonstrating the reliability of our structural models. We did not model the extended conformation of α_{IIb} ectodomain because of the lack of α_{IIb} and α_V crystal structures at the extended state.

Structure of the β_3 PSI domain at the bent and extended conformations

The β_3 PSI domain has been shown to have some functional relevance.[39,40] Of interest, a Leu33Pro polymorphism at the β_3 PSI domain forms the HPA-1a/b alloantigen.[15,17] The β_3 PSI domain also contains the epitope of active conformation-specific mAb AP5,[41] indicating its conformational changes upon β_3 activation. Leu33Pro locates at the C26-C38 loop of the PSI domain (Figure 4A-B). Previous studies have suggested that β_3 harboring Pro33 could be a risk factor for thrombosis because of the elevated function of $\alpha_{IIb}\beta_3$ in platelets, but the conclusions are controversial.[18-20] Our structures of the β_3 headpiece in both Leu33 and Pro33 forms as well as in the intermediate and extended states provide new structural information of the PSI domain.

Structural superimposition on the I-EGF1 domain showed that the overall conformations of the PSI and I-EGF1 domains were nearly identical between the intermediate and bent states of β_3 (Figure 4A). Interestingly, in the extended conformation, the C26-C38 loop of the PSI domain moved close to the I-EGF1 domain (Figure 4A). In addition, the C437-C448 loop of I-EGF1 domain also moved toward the PSI C26-C38 loop in the extended conformation (Figure 4A). These structural characters were observed in the cβ_3-E2 structures with either Pro33 or Leu33 (supplemental Figure 4C-D), demonstrating that Leu33-Pro substitution does not affect the local conformation of PSI domain.

Leu33Pro substitution does not elevate the ligand binding of β_3 integrin

The sequences of the C26-C38 loop are relatively conserved among different species, but variations are seen at the positions equivalent to β_3-Leu33 (Figure 4B). We examined whether the Leu33Pro polymorphism affects the activation of β_3 integrin. Ligand mimetic mAb PAC-1 was used to measure the activation of $\alpha_{IIb}\beta_3$ stimulated either by Mn^{2+} or by the cytoplasmic activating mutation α_{IIb}-R995A that mimics inside-out activation.[42] No differences in PAC-1 binding were observed between β_3-Leu33 and β_3-Pro33 (Figure 4C). Similarly, no difference was observed in PAC-1 binding to $\alpha_{IIb}\beta_3$-Leu33 and $\alpha_{IIb}\beta_3$-Pro33 induced by the overexpression of EGFP-tagged talin head domain (Figure 4D). Moreover, no difference was found

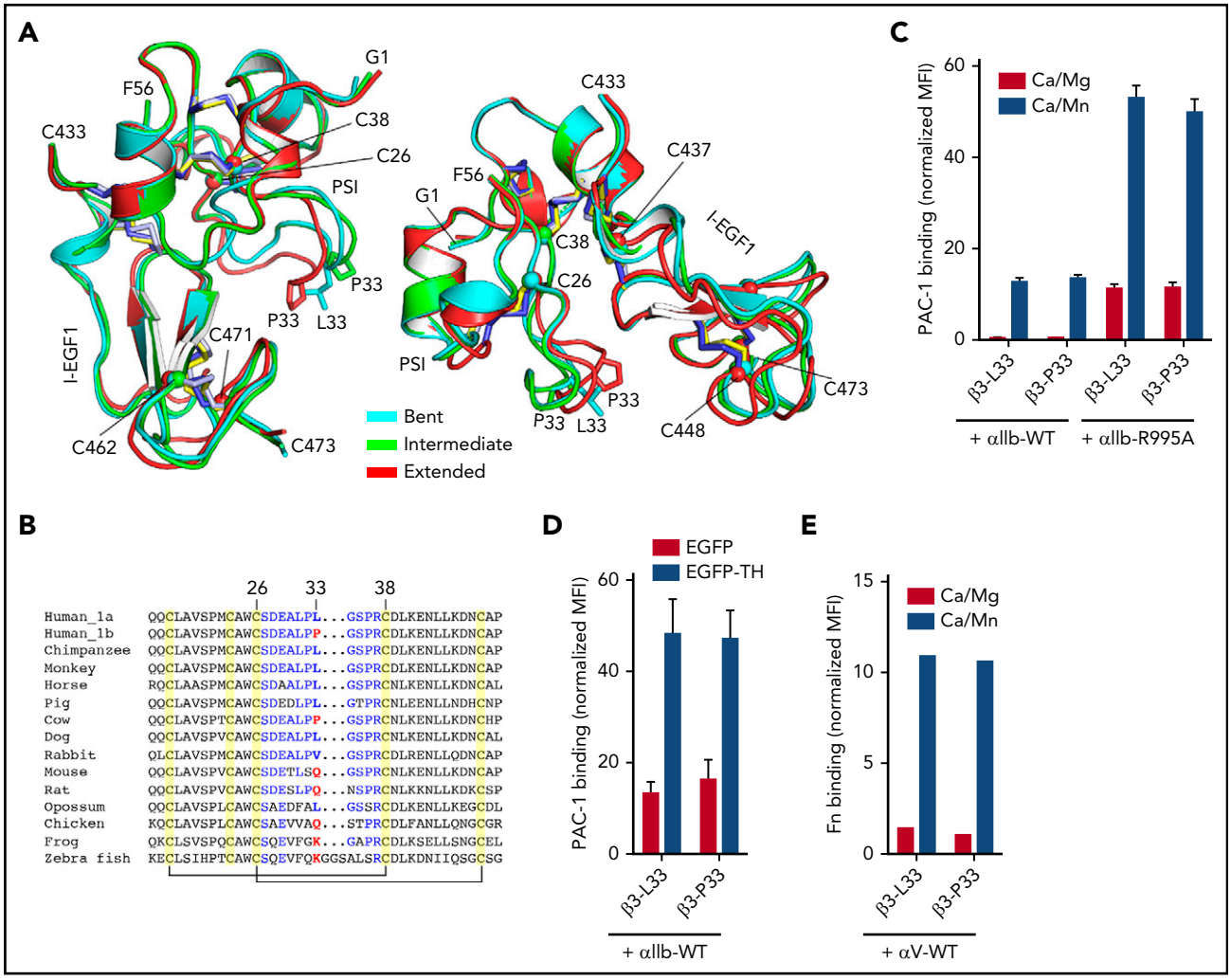

Figure 4. Structure of the β_3 PSI domain. (A) Two different views of the superposition of the bent (PDB 3FCS), intermediate, and extended β_3 structures on the PSI domain. Disulfide bonds, Pro33, and Leu33 are sticks. Selected cysteines are shown as Cα spheres. (B) Sequence alignment of a portion of the PSI domain containing the C26-C38 loop. Disulfide linkages are indicated. (C) Mn^{2+}-stimulated binding of the ligand mimetic mAb PAC-1 to HEK293FT cells transfected with the indicated α_{IIb} and β_3 constructs. PAC-1 binding was performed in the presence of 1 mM of Ca^{2+}/Mg^{2+} or 0.2 mM of Ca^{2+} plus 2 mM Mn^{2+}. (D) Talin head (TH)–induced PAC-1 binding to HEK293FT cells transfected with the indicated α_{IIb} and β_3 constructs plus EGFP or EGFP-TH. PAC-1 binding was performed in the presence of 1 mM of Ca^{2+}/Mg^{2+}. (E) Mn^{2+}-stimulated binding of fibronectin (Fn) to HEK293FT cells transfected with the indicated α_V and β_3 constructs. Fn binding was performed in the presence of 1 mM of Ca^{2+}/Mg^{2+} or 0.2 mM of Ca^{2+} plus 2 mM of Mn^{2+}. All the ligand binding results are presented as the mean fluorescence intensity (MFI) normalized to integrin expression. WT, wild type.

between β_3-Leu33 and β_3-Pro33 in Mn^{2+}-stimulated fibronectin binding to $\alpha_V\beta_3$ (Figure 4E). These data demonstrate that Pro33 does not render β_3 integrin more active than the Leu33 form.

A conserved arginine at the β subunit PSI/hybrid domain interface restrains integrin activation

The β_3 PSI domain connects with the hybrid domain through a short loop (Figure 5A). During the headpiece extension and hybrid domain swing-out, the PSI domain moves along with the hybrid domain (supplemental Figure 1C). We found no significant structural differences at the PSI/hybrid interface between the bent and extended β_3 headpieces (Figure 5A-B). The side chain of Arg93 at the hybrid domain A'B loop inserts into the hybrid/PSI interface and forms multiple hydrogen bonds with the backbone carbonyl oxygens of the PSI domain and the hybrid-PSI connecting loop (Figure 5A). These hydrogen bonds are maintained in the extended β_3 conformation (Figure 5B) and in the open headpiece of β_3.[6] Such hydrogen bond interactions may be critical in maintaining the rigidity of the hybrid/PSI interface. Of interest, the equivalent Arg is completely conserved among all the integrin β subunits (Figure 5C). Mutagenesis studies were performed to investigate the function of this conserved Arg in integrin activation. As shown by the ligand-binding assay, β_3-R93A and β_3-R93Q mutations remarkably augmented Mn^{2+}-stimulated PAC-1 binding to $\alpha_{IIb}\beta_3$ integrin, although the expression level was also greatly decreased (Figure 5D). Basal PAC-1 binding under the physiological Ca^{2+}/Mg^{2+} concentration was also increased by β_3-R93 mutations (Figure 5D). Consistently, the β_3-R93A mutation greatly enhanced fibronectin binding to $\alpha_V\beta_3$ (Figure 5E). Similar results were obtained for β_2 and β_1 integrins. The β_2-R87A mutation greatly enhanced ICAM-1 binding to $\alpha_L\beta_2$ (Figure 5F). β_1-R104A greatly enhanced fibronectin binding to $\alpha_5\beta_1$ (Figure 5G). Consistent with the fibronectin-binding assay, the β_1-R104A mutation enhanced both basal- and Mn^{2+}-stimulated binding of 9EG7 to $\alpha_5\beta_1$ (Figure 5H), demonstrating that disruption of the hybrid/PSI interface induces the extension of β_1 integrin.

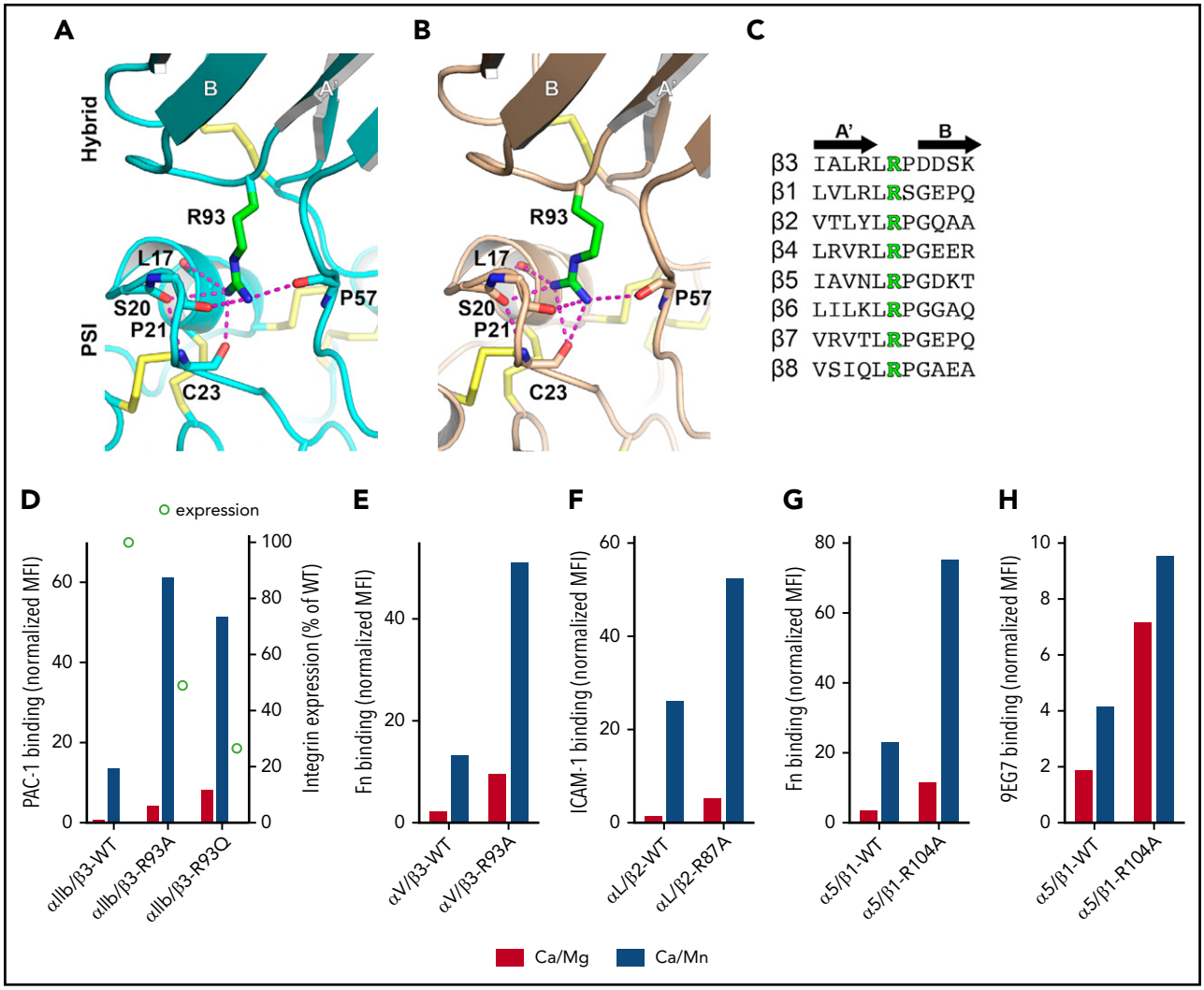

Figure 5. A conserved arginine at the hybrid-PSI interface. (A-B) The hybrid-PSI interface of bent (A) and extended (B) β_3. Disulfide bonds are yellow sticks. Hydrogen bonds are dashed in magenta. (C) Sequence alignment of the hybrid domain A'B loop. (D-H) PAC-1, ICAM-1, fibronectin (Fn), or 9EG7 binding of the β_3-R93 (D-E), β_2-R87 (F), or β_1-R104 (G-H) mutations coexpressed with α_{IIb} (D), α_V (E), α_L (F), or α_5 (G-H) integrin in HEK293FT cells. The binding was performed in the presence of 1 mM of Ca^{2+}/Mg^{2+} (Ca/Mg) or 0.2 mM of Ca^{2+} plus 2 mM Mn^{2+} (Ca/Mn) and is presented as mean fluorescence intensity (MFI) normalized to integrin expression. One representative result is shown. WT, wild type.

Discussion

Our high-resolution structural studies reveal how β_3 becomes extended at the I-EGF1/2 junction. Our data suggest that the multiple conformational states of β_3 observed in many EM studies[5,8-11,43-45] could be afforded by the conformational plasticity of the I-EGF2 C1-C2 loop. Previous studies have demonstrated that the length of the I-EGF2 C1-C2 loop modulates β_3 integrin activation.[46] The long and short loops favor the resting and active states, respectively.[46] The C1-C2 loop of I-EGF2 was the longest among the I-EGF domains. The I-EGF3 C1-C2 loop had 6 residues, whereas the I-EGF4 C1-C2 loop had 4 residues. The angle between I-EGF3 and I-EGF4 was closer to straight than the others (Figure 2G-H). The C1-C2 loop of β_2 I-EGF2 had 13 residues (Figure 2F). Consistently, the β_2 I-EGF1/2 junction was less extended than that of β_3, which had 12 residues spanning the C1-C2 loop (Figure 2F). These structural features of I-EGF domains are compatible with the long-range conformational changes of integrin. The rigidity of I-EGF2/3 and I-EGF3/4 interfaces provides a support for the extension of the integrin headpiece and for the resistance of mechanical force.[5] The flexibility of the I-EGF1/2 interface allows the headpiece to pose at different conformations, which is required for affinity regulation. Given the critical role of the I-EGF2 C1-C2 loop in integrin extension, an intriguing strategy would be to target the C1-C2 loop, such as by antibodies, which may modulate integrin conformational change and cellular function.

Our structural studies have important implications for integrin conformational activation. Integrin headpiece extension is afforded by the extension of the β subunit at the I-EGF1/2 junction (β knee) and the extension of the α subunit at the thigh/calf-1 junction (α knee; Figure 3B-F; supplemental Figure 1). Because of the large interface formed between the β-propeller and βI domains, the α and β extensions need to occur simultaneously. Our high-resolution structures of β_3-knee at intermediate and extended conformations demonstrate the flexibility of this region. Extension of the I-EGF1 domain did not generate new interactions at the I-EGF1/2 junction (Figure 3D). Indeed, only a very small interface formed at the β_3 I-EGF1/2 junction, even in the bent conformation (Figure 3B). By contrast,

the thigh/calf-1 junction in bent α_{IIb} formed a larger interface composed of hydrogen bonds and hydrophobic interactions (Figure 3G). This suggests that the bent α_{IIb} knee may resist the force of extension more than β_3 knee. EM and our modeled structure show that the α_{IIb} and α_V subunits can adopt an intermediate (half-extended) conformation (Figure 3B). After complete extension, α knee becomes straight and the thigh and calf-1 domains are expected to form new close contacts at their junction. Unlike extended β_3 knee, the new interface of extended α knee is expected to be rigid. These structural features are important for the conformational regulation of integrin by cytoskeletal force under conditions of cell adhesion and migration.[5,47,48] The flexibility of an extended β subunit afforded by the flexible I-EGF1/2 junction is required to sense and resist the changes of cellular forces, whereas the rigidity of an extended α leg may provide support for the sensing and resisting of tensile force by the β subunit.[47,49-51]

Local conformational changes were observed at the PSI and I-EGF1 domains upon β_3 extension. It is not readily known whether such conformational changes are functionally significant. Nonetheless, structural diversities of the PSI and I-EGF1 domains, especially at the C26-C38 loop, have been observed among the reported β_3 crystal structures (A.M.M.T., Z.W., D.Z., Y.Z., Brian R. Curtis, and J.Z., manuscript submitted April 2018). Moreover, the biological relevance of such conformational diversities is implicated by the binding of heterogeneous anti–HPA-1a alloantibodies. All anti–HPA-1a alloantibodies require Leu33 at the β_3 PSI C26-C38 loop.[16,17] However, some anti–HPA-1a alloantibodies require noncontiguous sequences and the integrity of the PSI domain to form the HPA-1a epitope.[52-56] In particular, certain anti–HPA-1a alloantibodies require both the PSI and I-EGF1 domains.[52,56,57] We have unpublished data demonstrating that the specific residues of the I-EGF1 domain are required for the binding of certain anti–HPA-1 alloantibodies. Of significance, recent studies have demonstrated that a subtype of maternal anti–HPA-1a alloantibodies could distinguish the $\alpha_{IIb}\beta_3$ vs $\alpha_V\beta_3$ complex.[58] $\alpha_V\beta_3$-specific anti–HPA-1a alloantibodies were indicated to be the cause of intracranial hemorrhages in fetus and neonates through the blockage of the $\alpha_V\beta_3$ function in endothelial cells.[58] We have data showing that $\alpha_{IIb}\beta_3$-specific anti–HPA-1a alloantibodies can specifically recognize the bent but not extended conformation of β_3 (A.M.M.T., Z.W., D.Z., Y.Z., Brian R. Curtis, and J.Z., manuscript submitted April 2018). In addition, a recent study showed that EDTA treatment of $\alpha_{IIb}\beta_3$, known to disturb $\alpha_{IIb}\beta_3$ conformation,[41,59-61] reduced the binding of anti–HPA-1a.[62] All these data suggest the conformation-dependent feature of anti–HPA-1a alloantibodies. The conformational changes of the PSI and I-EGF1 domains observed in our extended β_3 structure may account for the differences in anti–HPA-1a binding.

It is remarkable that the anti–HPA-1a alloantibodies could distinguish the subtle conformational differences of the PSI and I-EGF1 domains. More interestingly, some but not all anti–HPA-1a alloantibodies were found to block the function of $\alpha_{IIb}\beta_3$ and/or $\alpha_V\beta_3$ integrins.[58,63] Our current studies provide a structure-based interpretation for this observation. The conformational differences of the PSI and I-EGF1 domains may determine the binding poses of the alloantibodies, which in turn exert either a blocking or nonblocking effect on β_3 function. In particular, the bent conformation-dependent anti–HPA-1a alloantibodies may block the integrin function by stabilizing β_3 in the bent conformation. This raises an intriguing possibility that the inhibitory antibodies targeting the PSI and I-EGF1 domains may be developed to specifically target $\alpha_{IIb}\beta_3$ or $\alpha_V\beta_3$ integrin.

Polymorphism substitution β_3-R93Q has been shown to disrupt the binding of certain anti–HPA-1a (β_3-Leu33) alloantibodies.[64] β_3-R93 is more than 28-Å distal from β_3-Leu33 and is buried into the hybrid/PSI interface, and thus cannot directly participate in the HPA-1a epitope. Here, we found that β_3-R93 mutations induced the active conformation of β_3 integrin, which may have led to the structural changes of the PSI C26-C38 loop and the I-EGF1 domain as observed in our extended β_3 structure (Figure 4A). As discussed, such conformational changes may alter the binding of anti–HPA-1a alloantibodies.

We found no differences in either conformation or ligand binding between the Leu33 and Pro33 forms of β_3. Studies using human platelets or cell lines have shown that β_3-Pro33 enhanced cell adhesion and outside-in signaling.[18,65-68] A recent study using knock-in mice showed the Pro33 form of mouse β_3 increased platelet adhesion, clot formation, and aggregation, probably as a result of elevated Src activation.[69] However, agonist-induced soluble ligand binding was not affected, consistent with our data. Interestingly, the talin association with mouse β_3 was also increased by the presence of Pro33.[69] Because Pro33 does not directly alter the conformation of the PSI domain (Figure 4A), it remains unknown by which mechanism Pro33 affects β_3 function. Molecular dynamics simulation studies have indicated that Pro33 substitution might affect β_3 function by modifying the structural equilibrium of the PSI and the I-EGF domains and probably integrin extension,[70,71] but such an effect may not directly affect ligand binding according to our study.

Acknowledgments

The authors thank Peter Newman for helpful discussions and for providing antibodies.

This work was supported by grants HL122985 and HL131836 (J.Z.) from the National Heart, Lung, and Blood Institute of the National Institutes of Health.

Authorship

Contribution: D.Z. collected X-ray diffraction data and refined the structures; A.M.M.T. performed functional assays and collected X-ray diffraction data; Y.Z. contributed to protein purification; Z.W. contributed to the generation of DNA constructs; J.Z. designed the study, did protein crystallography, and wrote the manuscript; and all authors contributed to manuscript preparation.

Conflict-of-interest disclosure: The authors declare no competing financial interests.

Correspondence: Jieqing Zhu, Blood Research Institute, BloodCenter of Wisconsin, 8727 Watertown Plank Rd, Milwaukee, WI 53226; e-mail: jieqing.zhu@bcw.edu.

Footnotes

Submitted 26 January 2018; accepted 10 July 2018. Prepublished online as *Blood* First Edition paper, 17 July 2018; DOI 10.1182/blood-2018-01-829572.

The online version of this article contains a data supplement.

The publication costs of this article were defrayed in part by page charge payment. Therefore, and solely to indicate this fact, this article is hereby marked "advertisement" in accordance with 18 USC section 1734.

REFERENCES

1. Hynes RO. Integrins: bidirectional, allosteric signaling machines. *Cell*. 2002;110(6):673-687.
2. Springer TA, Dustin ML. Integrin inside-out signaling and the immunological synapse. *Curr Opin Cell Biol*. 2012;24(1):107-115.
3. Xiong JP, Stehle T, Zhang R, et al. Crystal structure of the extracellular segment of integrin α Vbeta3 in complex with an Arg-Gly-Asp ligand. *Science*. 2002;296(5565):151-155.
4. Xiong J-P, Stehle T, Diefenbach B, et al. Crystal structure of the extracellular segment of integrin α Vbeta3. *Science*. 2001;294(5541):339-345.
5. Zhu J, Luo BH, Xiao T, Zhang C, Nishida N, Springer TA. Structure of a complete integrin ectodomain in a physiologic resting state and activation and deactivation by applied forces. *Mol Cell*. 2008;32(6):849-861.
6. Xiao T, Takagi J, Coller BS, Wang JH, Springer TA. Structural basis for allostery in integrins and binding to fibrinogen-mimetic therapeutics. *Nature*. 2004;432(7013):59-67.
7. Takagi J, Petre BM, Walz T, Springer TA. Global conformational rearrangements in integrin extracellular domains in outside-in and inside-out signaling. *Cell*. 2002;110(5):599-611.
8. Ye F, Hu G, Taylor D, et al. Recreation of the terminal events in physiological integrin activation. *J Cell Biol*. 2010;188(1):157-173.
9. Choi WS, Rice WJ, Stokes DL, Coller BS. Three-dimensional reconstruction of intact human integrin αIIbβ3: new implications for activation-dependent ligand binding. *Blood*. 2013;122(26):4165-4171.
10. Xu XP, Kim E, Swift M, Smith JW, Volkmann N, Hanein D. Three-dimensional structures of full-length, membrane-embedded human $\alpha_{(IIb)}\beta_{(3)}$ integrin complexes. *Biophys J*. 2016;110(4):798-809.
11. Eng ET, Smagghe BJ, Walz T, Springer TA. Intact alphaIIbbeta3 integrin is extended after activation as measured by solution X-ray scattering and electron microscopy. *J Biol Chem*. 2011;286(40):35218-35226.
12. Coller BS. $\alpha_{IIb}\beta_3$: structure and function. *J Thromb Haemost*. 2015;13(suppl 1):S17-S25.
13. Atkinson SJ, Ellison TS, Steri V, Gould E, Robinson SD. Redefining the role(s) of endothelial $\alpha_v\beta_3$-integrin in angiogenesis. *Biochem Soc Trans*. 2014;42(6):1590-1595.
14. Seguin L, Desgrosellier JS, Weis SM, Cheresh DA. Integrins and cancer: regulators of cancer stemness, metastasis, and drug resistance. *Trends Cell Biol*. 2015;25(4):234-240.
15. Newman PJ, Derbes RS, Aster RH. The human platelet alloantigens, PlA1 and PlA2, are associated with a leucine33/proline33 amino acid polymorphism in membrane glycoprotein IIIa, and are distinguishable by DNA typing. *J Clin Invest*. 1989;83(5):1778-1781.
16. Sachs UJ. Fetal/neonatal alloimmune thrombocytopenia. *Thromb Res*. 2013;131(suppl 1):S42-S46.
17. Curtis BR. Recent progress in understanding the pathogenesis of fetal and neonatal alloimmune thrombocytopenia. *Br J Haematol*. 2015;171(5):671-682.
18. Vijayan KV, Goldschmidt-Clermont PJ, Roos C, Bray PF. The Pl(A2) polymorphism of integrin $\beta_{(3)}$ enhances outside-in signaling and adhesive functions. *J Clin Invest*. 2000;105(6):793-802.
19. Byzova TV, Plow EF. The Pl(A2) allele and cardiovascular disease: the pro(33) and con. *J Clin Invest*. 2000;105(6):697-698.
20. Bennett JS, Catella-Lawson F, Rut AR, et al. Effect of the Pl(A2) alloantigen on the function of $\beta_{(3)}$-integrins in platelets. *Blood*. 2001;97(10):3093-3099.
21. Cai X, Thinn AMM, Wang Z, Shan H, Zhu J. The importance of N-glycosylation on β_3 integrin ligand binding and conformational regulation. *Sci Rep*. 2017;7(1):4656.
22. Liu J, Wang Z, Thinn AM, Ma YQ, Zhu J. The dual structural roles of the membrane distal region of the α-integrin cytoplasmic tail during integrin inside-out activation. *J Cell Sci*. 2015;128(9):1718-1731.
23. Zhang C, Liu J, Jiang X, et al. Modulation of integrin activation and signaling by α1/α1′-helix unbending at the junction. *J Cell Sci*. 2013;126(Pt 24):5735-5747.
24. Mi LZ, Grey MJ, Nishida N, Walz T, Lu C, Springer TA. Functional and structural stability of the epidermal growth factor receptor in detergent micelles and phospholipid nanodiscs. *Biochemistry*. 2008;47(39):10314-10323.
25. Battye TG, Kontogiannis L, Johnson O, Powell HR, Leslie AG. iMOSFLM: a new graphical interface for diffraction-image processing with MOSFLM. *Acta Crystallogr D Biol Crystallogr*. 2011;67(Pt 4):271-281.
26. McCoy AJ, Grosse-Kunstleve RW, Adams PD, Winn MD, Storoni LC, Read RJ. Phaser crystallographic software. *J Appl Cryst*. 2007;40(Pt 4):658-674.
27. Emsley P, Lohkamp B, Scott WG, Cowtan K. Features and development of Coot. *Acta Crystallogr D Biol Crystallogr*. 2010;66(Pt 4):486-501.
28. Adams PD, Afonine PV, Bunkóczi G, et al. PHENIX: a comprehensive Python-based system for macromolecular structure solution. *Acta Crystallogr D Biol Crystallogr*. 2010;66(Pt 2):213-221.
29. Lenter M, Uhlig H, Hamann A, Jenö P, Imhof B, Vestweber D. A monoclonal antibody against an activation epitope on mouse integrin chain β 1 blocks adhesion of lymphocytes to the endothelial integrin alpha 6 β 1. *Proc Natl Acad Sci USA*. 1993;90(19):9051-9055.
30. Askari JA, Tynan CJ, Webb SE, Martin-Fernandez ML, Ballestrem C, Humphries MJ. Focal adhesions are sites of integrin extension. *J Cell Biol*. 2010;188(6):891-903.
31. Springer TA. Complement and the multifaceted functions of VWA and integrin I domains. *Structure*. 2006;14(11):1611-1616.
32. Lee JO, Rieu P, Arnaout MA, Liddington R. Crystal structure of the A domain from the α subunit of integrin CR3 (CD11b/CD18). *Cell*. 1995;80(4):631-638.
33. Takagi J, Debottis DP, Erickson HP, Springer TA. The role of specificity-determining loop of the integrin β-subunit I-like domain in folding, association with the α subunit, and ligand binding. *Biochemistry*. 2002;41(13):4339-4347.
34. Shimaoka M, Xiao T, Liu J-H, et al. Structures of the α_L I domain and its complex with ICAM-1 reveal a shape-shifting pathway for integrin regulation. *Cell*. 2003;112(1):99-111.
35. Dong X, Mi LZ, Zhu J, et al. $\alpha_{(V)}\beta_{(3)}$ integrin crystal structures and their functional implications. *Biochemistry*. 2012;51(44):8814-8828.
36. Shi M, Foo SY, Tan SM, Mitchell EP, Law SK, Lescar J. A structural hypothesis for the transition between bent and extended conformations of the leukocyte β_2 integrins. *J Biol Chem*. 2007;282(41):30198-30206.
37. Sen M, Yuki K, Springer TA. An internal ligand-bound, metastable state of a leukocyte integrin, $\alpha_X\beta_2$. *J Cell Biol*. 2013;203(4):629-642.
38. Zhu J, Zhu J, Negri A, et al. Closed headpiece of integrin αIIbβ3 and its complex with an αIIbβ3-specific antagonist that does not induce opening. *Blood*. 2010;116(23):5050-5059.
39. Raymond T, Gorbunova E, Gavrilovskaya IN, Mackow ER. Pathogenic hantaviruses bind plexin-semaphorin-integrin domains present at the apex of inactive, bent alphavbeta3 integrin conformers. *Proc Natl Acad Sci USA*. 2005;102(4):1163-1168.
40. Zhu G, Zhang Q, Reddy EC, et al. The integrin PSI domain has an endogenous thiol isomerase function and is a novel target for antiplatelet therapy. *Blood*. 2017;129(13):1840-1854.
41. Honda S, Tomiyama Y, Pelletier AJ, et al. Topography of ligand-induced binding sites, including a novel cation-sensitive epitope (AP5) at the amino terminus, of the human integrin β_3 subunit. *J Biol Chem*. 1995;270(20):11947-11954.
42. Hughes PE, Diaz-Gonzalez F, Leong L, et al. Breaking the integrin hinge. A defined structural constraint regulates integrin signaling. *J Biol Chem*. 1996;271(12):6571-6574.
43. Weisel JW, Nagaswami C, Vilaire G, Bennett JS. Examination of the platelet membrane glycoprotein IIb-IIIa complex and its interaction with fibrinogen and other ligands by electron microscopy. *J Biol Chem*. 1992;267(23):16637-16643.
44. Adair BD, Yeager M. Three-dimensional model of the human platelet integrin α IIbbeta 3 based on electron cryomicroscopy and x-ray crystallography. *Proc Natl Acad Sci USA*. 2002;99(22):14059-14064.
45. Ye F, Liu J, Winkler H, Taylor KA. Integrin $\alpha_{IIb}\beta_3$ in a membrane environment remains the same height after Mn^{2+} activation when observed by cryoelectron tomography. *J Mol Biol*. 2008;378(5):976-986.
46. Smagghe BJ, Huang PS, Ban Y-E, Baker D, Springer TA. Modulation of integrin activation

by an entropic spring in the β-knee. *J Biol Chem*. 2010;285(43):32954-32966.

47. Nordenfelt P, Elliott HL, Springer TA. Coordinated integrin activation by actin-dependent force during T-cell migration. *Nat Commun*. 2016;7:13119.

48. Swaminathan V, Kalappurakkal JM, Mehta SB, et al. Actin retrograde flow actively aligns and orients ligand-engaged integrins in focal adhesions. *Proc Natl Acad Sci USA*. 2017; 114(40):10648-10653.

49. Oria R, Wiegand T, Escribano J, et al. Force loading explains spatial sensing of ligands by cells. *Nature*. 2017;552(7684):219-224.

50. Li J, Springer TA. Integrin extension enables ultrasensitive regulation by cytoskeletal force. *Proc Natl Acad Sci USA*. 2017;114(18): 4685-4690.

51. Chowdhury F, Li ITS, Leslie BJ, et al. Single molecular force across single integrins dictates cell spreading. *Integr Biol*. 2015;7(10): 1265-1271.

52. Honda S, Honda Y, Bauer B, Ruan C, Kunicki TJ. The impact of three-dimensional structure on the expression of PlA alloantigens on human integrin β 3. *Blood*. 1995;86(1):234-242.

53. Valentin N, Visentin GP, Newman PJ. Involvement of the cysteine-rich domain of glycoprotein IIIa in the expression of the human platelet alloantigen, PlA1: evidence for heterogeneity in the humoral response. *Blood*. 1995;85(11):3028-3033.

54. Liu LX, Nardi MA, Casella JF, Karpatkin S. Inhibition of binding of anti-PLA1 antibodies to platelets with monoclonal antibody LK-4. Evidence for multiple PLA1 receptor sites on platelet GPIIIa. *Blood*. 1996;88(9):3601-3607.

55. Barron-Casella EA, Nebbia G, Rogers OC, King KE, Kickler TS, Casella JF. Construction of a human platelet alloantigen-1a epitope(s) within murine glycoprotein IIIa: identification of residues critical to the conformation of the antibody binding site(s). *Blood*. 1999;93(9): 2959-2967.

56. Stafford P, Ghevaert C, Campbell K, et al. Immunologic and structural analysis of eight novel domain-deletion β_3 integrin peptides designed for detection of HPA-1 antibodies. *J Thromb Haemost*. 2008;6(2):366-375.

57. Sun Q-H, Liu CY, Wang R, Paddock C, Newman PJ. Disruption of the long-range GPIIIa Cys(5)-Cys(435) disulfide bond results in the production of constitutively active GPIIb-IIIa ($\alpha_{(IIb)}\beta_{(3)}$) integrin complexes. *Blood*. 2002; 100(6):2094-2101.

58. Santoso S, Wihadmadyatami H, Bakchoul T, et al. Antiendothelial $\alpha_v\beta_3$ antibodies are a major cause of intracranial bleeding in fetal/neonatal alloimmune thrombocytopenia. *Arterioscler Thromb Vasc Biol*. 2016;36(8): 1517-1524.

59. White JG. EDTA-induced changes in platelet structure and function: clot retraction. *Platelets*. 2000;11(1):49-55.

60. Ginsberg MH, Lightsey A, Kunicki TJ, Kaufmann A, Marguerie G, Plow EF. Divalent cation regulation of the surface orientation of platelet membrane glycoprotein IIb. Correlation with fibrinogen binding function and definition of a novel variant of Glanzmann's thrombasthenia. *J Clin Invest*. 1986;78(4): 1103-1111.

61. Zafar H, Shang Y, Li J, et al. $\alpha_{IIb}\beta_3$ binding to a fibrinogen fragment lacking the γ-chain dodecapeptide is activation dependent and EDTA inducible. *Blood Adv*. 2017;1(7): 417-428.

62. Allen DL, Abrahamsson S, Murphy MF, Roberts DJ. Human platelet antigen 1a epitopes are dependent on the cation-regulated conformation of integrin $\alpha_{(IIb)}\beta_{(3)}$ (GPIIb/IIIa). *J Immunol Methods*. 2012;375(1-2):166-175.

63. Kroll H, Penke G, Santoso S. Functional heterogeneity of alloantibodies against the human platelet antigen (HPA)-1a. *Thromb Haemost*. 2005;94(6):1224-1229.

64. Watkins NA, Schaffner-Reckinger E, Allen DL, et al. HPA-1a phenotype-genotype discrepancy reveals a naturally occurring Arg93Gln substitution in the platelet β_3 integrin that disrupts the HPA-1a epitope. *Blood*. 2002;99(5):1833-1839.

65. Vijayan KV, Liu Y, Sun W, Ito M, Bray PF. The Pro33 isoform of integrin β_3 enhances outside-in signaling in human platelets by regulating the activation of serine/threonine phosphatases. *J Biol Chem*. 2005;280(23): 21756-21762.

66. Vijayan KV, Huang TC, Liu Y, et al. Shear stress augments the enhanced adhesive phenotype of cells expressing the Pro33 isoform of integrin β_3. *FEBS Lett*. 2003;540(1-3):41-46.

67. Vijayan KV, Liu Y, Dong JF, Bray PF. Enhanced activation of mitogen-activated protein kinase and myosin light chain kinase by the Pro33 polymorphism of integrin β 3. *J Biol Chem*. 2003;278(6):3860-3867.

68. Sajid M, Vijayan KV, Souza S, Bray PF. PlA polymorphism of integrin β 3 differentially modulates cellular migration on extracellular matrix proteins. *Arterioscler Thromb Vasc Biol*. 2002;22(12):1984-1989.

69. Oliver KH, Jessen T, Crawford EL, Chung CY, Sutcliffe JS, Carneiro AM. Pro32Pro33 mutations in the integrin β_3 PSI domain result in $\alpha_{IIb}\beta_3$ priming and enhanced adhesion: reversal of the hypercoagulability phenotype by the Src inhibitor SKI-606. *Mol Pharmacol*. 2014;85(6):921-931.

70. Jallu V, Poulain P, Fuchs PF, Kaplan C, de Brevern AG. Modeling and molecular dynamics of HPA-1a and -1b polymorphisms: effects on the structure of the β_3 subunit of the $\alpha_{IIb}\beta_3$ integrin. *PLoS One*. 2012;7(11):e47304.

71. Pagani G, Pereira JPV, Stoldt VR, Beck A, Scharf RE, Gohlke H. The human platelet antigen-1b (Pro^{33}) variant of $\alpha_{IIb}\beta_3$ allosterically shifts the dynamic conformational equilibrium of this integrin toward the active state. *J Biol Chem*. 2018;293(13):4830-4844.